Design, Implementation, and Experimental Results of a Quaternion-Based Kalman Filter for Human Body Motion Tracking

Xiaoping Yun, *Fellow, IEEE*, and Eric R. Bachmann, *Member, IEEE*

***Abstract*—Real-time tracking of human body motion is an important technology in synthetic environments, robotics, and other human–computer interaction applications. This paper presents an extended Kalman filter designed for real-time estimation of the orientation of human limb segments. The filter processes data from small inertial/magnetic sensor modules containing triaxial angular rate sensors, accelerometers, and magnetometers. The filter represents rotation using quaternions rather than Euler angles or axis/angle pairs. Preprocessing of the acceleration and magnetometer measurements using the Quest algorithm produces a computed quaternion input for the filter. This preprocessing reduces the dimension of the state vector and makes the measurement equations linear. Real-time implementation and testing results of the quaternion-based Kalman filter are presented. Experimental results validate the filter design, and show the feasibility of using inertial/magnetic sensor modules for real-time human body motion tracking.**

***Index Terms*—Inertial sensors, Kalman filtering, magnetic sensors, motion measurement, orientation tracking, pose estimation, quaternions, virtual reality.**

I. Introduction

MOTION tracking is a key technology in synthetic environments, robotics, and other applications that require real-time information about the motion of a human. A number of motion-tracking technologies have been developed for human motion capture in virtual reality and biomedical applications, including mechanical trackers, active magnetic trackers, optical tracking systems, acoustic, and inertial/magnetic tracking systems. Most are dependent on an artificially generated source and are thus range-limited and susceptible to interference and noise.

Mechanical tracking systems can be placed in two separate categories. Body-based systems use an exoskeleton that is attached to the articulated structure to be tracked [1]. Goniometers within the skeletal linkages measure joint angles. Ground-based systems attach one end of a boom or shaft to a tracked object and typically have six degrees of freedom (DOFs) [2]. Ground-based systems normally only track a single rigid body, but have the advantage of being able to provide haptic feedback.

Practical optical tracking systems can also be separated into two basic categories. Pattern recognition systems sense an artificial pattern of lights and use this information to determine position and/or orientation [3]. Such systems may be "outside-in" when the sensors are fixed and the emitters are mobile, or "inside-out" when sensors are mounted on mobile objects and the emitters are fixed. Image-based systems determine position by using multiple cameras to track predesignated points on moving objects within a working volume. The tracked points may be marked actively or passively [4], [5].

Active magnetic tracking systems determine both position and orientation by using sets of small orthogonally mounted coils to sense a set of sequentially generated magnetic fields. The sequentially emitted fields induce current in each of the sensor coils, allowing measurement of orientation. Changes in total strength across the sensor coils are proportional to the distance from the field transmitter and can be used to measure position [6].

Ultrasonic tracking systems can determine position through either time-of-flight and triangulation or phase-coherence. Phase-coherence trackers determine distance by measuring the difference in phase of a reference signal and an emitted signal detected by sensors.

Body tracking using inertial and magnetic sensors is a relatively new technology. Inertial/magnetic tracking is appealing due to a lack of dependence on an artificially generated source. It thus does not suffer from range limitations and interference problems of sourced technologies. All delay or latency is due to data processing and transmission. The availability of low-cost, small-size micro-electro-mechanical systems (MEMS) sensors has made it possible to build wrist-watch-sized, self-contained inertial/magnetic sensor modules [7], [8]. These modules can be used to accurately track orientation in real time. Attachment of such sensor modules to each of the major limb segments of a human makes it possible to independently determine the orientation of each segment relative to an Earth-fixed reference frame. The human model is constructed from multiple independently oriented limb segments that are constrained by their attachment to each other. Relative orientation between limb segments is not determined or needed.

A naive approach to inertial orientation tracking might involve integration of angular rate data to determine orientation. However, this solution would be prone to drift over time due to

Manuscript received December 22, 2005; revised June 15, 2006. This paper was recommended for publication by Associate Editor J. Tardos and Editor H. Arai upon evaluation of the reviewers' comments. This work was supported in part by the Army Research Office (ARO), and in part by the Navy Modeling and Simulation Management Office (NMSO). This paper was presented in part at the IEEE International Conference on Robotics and Automation, Barcelona, Spain, April 2005.

X. Yun is with the Department of Electrical and Computer Engineering, Naval Postgraduate School, Monterey, CA 93943 USA (e-mail: yun@ieee.org).

E. R. Bachmann is with the Department of Computer Science and System Analysis, Miami University, Oxford, OH 45056 USA.

Digital Object Identifier 10.1109/TRO.2006.886270

the buildup of bias and drift errors. In order to avoid drift, inertial tracking systems make use of additional complementary sensors. Commonly, these sensors include triads of accelerometers and magnetometers for respectively referencing the gravity and magnetic field vectors. Measuring the gravity vector in the sensor coordinate frame using accelerometers allows estimation of orientation relative to the horizontal plane. However, in the event that the sensor module is rotated about the vertical axis, the projection of the gravity vector on each of the principal axes of the accelerometer triad will not change. Since the accelerometer triad can not be used to sense a rotation about the vertical axis, magnetometers are used to measure the local magnetic field vector in sensor coordinates and allows determination of orientation relative to the vertical. The data from the incorporated sensors is normally fused using a Kalman or complementary filtering algorithm. It should be noted that data from low-cost MEMS accelerometers cannot be double-integrated for an extended period of time to determine position, due to a quadratic growth of errors.

This paper describes the design, implementation, and experimental testing of an extended Kalman filter (EKF) for real-time tracking of human body motion. In order to produce 3-D orientation estimates relative to an Earth-fixed reference frame, the filter uses input data from a sensor module containing a triad of orthogonally mounted linear accelerometers, a triad of orthogonally mounted angular rate sensors, and a triad of orthogonally mounted magnetometers. Quaternions are used to represent orientation to improve computational efficiency and avoid singularities. In addition, the use of quaternions eliminates the need for computing trigonometric functions. The filter continuously corrects for drift based on the assumption that human limb acceleration is bounded, and averages to zero over any extended period of time. A first-order linear system is used to model human body limb segment motion. The QUEST algorithm is used to preprocess accelerometer and magnetometer measurements, resulting in a significant simplification of the Kalman filter design. The filter is experimentally validated using actual sensor measurements.

The primary contributions of this paper are:

- analysis that determines that a simple motion model based on a first-order linear system is sufficient for tracking human limb segment orientation;
- an EKF designed for tracking human limb segment orientation that fuses a precalculated quaternion input with angular rate data;
- experimental results validating that filter performance is adequate for human posture tracking applications.

The paper is organized as follows. Section II provides an overview of related work, and contrasts that with the approach described in this paper. Section III gives a brief description of the MARG sensors used to obtain experimental data. Section IV presents the process model of the Kalman filter for human body motion tracking. Section V describes two approaches to Kalman filter design. Section VI describes implementation issues of the Kalman filter with a focus on how the nonlinear process model was first linearized and then discretized. Experimental modeling of the process noise covariance matrix and the measurement noise covariance matrix is also detailed. Section VII reports the MATLAB simulation and offline testing results of the Kalman filter. Section VIII describes the real-time implementation of the algorithm and testing results. The final section provides a summary and conclusions.

II. Related Work

Many studies of human motion tracking using inertial sensors have been performed. Depending on the type, number, and configuration of sensors used, some studies are limited to tracking two degrees of orientation in a plane, while others track 3-D orientation. Algorithms have also been designed to track limb segment orientations relative to each other or calculate joint angles, as opposed to estimating the orientation of a limb segment relative to an Earth-fixed reference frame.

A study of human motion tracking using accelerometers alone was reported in [9]. During motions involving small linear accelerations, a set of triaxial accelerometers was used to determine joint angles. During motions accompanied by higher accelerations, a technique is described that involves the use of two sets of triaxial accelerometers on a single rigid body to differentiate gravitational acceleration from motion-related linear acceleration. Though the effects of these geometric sensor fusion techniques are depicted, there is no comparison with truth data. The use of magnetometers is mentioned, but not discussed. Rehbinder and Hu [10] describe an attitude estimation algorithm based on the use of angular rate sensors and accelerometers. In this paper, drift in heading estimation was unavoidable due to a lack of additional complementary sensors, such as magnetometers. Thus, only two DOFs of orientation are tracked. Sabatini *et al.* [11] used a single sensor module containing a biaxial accelerometer and one gyroscope to perform gait analysis and measurement. To measure incline, distance, and speed, the method exploits the cyclical features of human gait. Transition from one gait phase to the next is determined using gyroscope data. Acceleration data is double integrated during the swing phase to determine position and used to determine the vertical when the foot is flat on the ground. Since the accelerometers are unable to detect rotations about the vertical plane, all motion is assumed to take place in a nonrotating sagittal plane. Sabatini [12] took this research further by creating a quaternion-based filtering algorithm. A quaternion interpolation technique is used to improve the accuracy of orientation and position estimates by reducing the effects of sensor bias and scale factor drift in both the accelerometers and gyroscope. Unlike the work described in this paper, this gait analysis work does not attempt to measure posture. In similar gait measurement work, Veltink *et al.* [13] use a sensor module containing a three-axis accelerometer and a three-axis angular rate sensor to measure gait characteristics in order to tune an implantable drop-foot simulator.

In a study of dynamic registration in augmented reality applications that require more precise orientation tracking as well as position tracking, Azuma and Bishop [14] use inertial data from linear accelerometers and angular rate sensors to reduce apparent lag in the position and orientation estimates produced by an optoelectronic tracking system. The use of an EKF predictor resulted in errors 5–10 times lower than without predic-

tion. In contrast, the work described in this paper produces only estimates of orientation using inertial and magnetic data.

Full 3-DOF orientation tracking is most commonly performed using nine-axis sensor modules containing three orthogonally mounted triads of angular rate sensors, accelerometers, and magnetometers. Foxlin *et al.* [15], [16] describes two commercial nine-axis sensing systems designed for head tracking applications. Sensor fusion is performed using a complementary separate-bias Kalman filter. Drift correction is described as only being performed during stationary periods when it is assumed accelerometers are sensing only gravitational acceleration. Thus, the described algorithm requires that all motion stop in order to correct inertial drift errors.

Bachmann *et al.* [7], [17] proposed a nonoptimal quaternion-based complementary filter for human body tracking. The filter is able to track through all orientations without singularities, and continuously correct for drift without a need for stationary periods using nine-axis inertial/magnetic sensor module data. Extensions to this work and the development of an optimal filter designed for human posture tracking applications are described in [18]–[20]. Use of a first-order linear system for modeling human body limb motions was first proposed in [18]. A Gauss–Newton iteration method is used to preprocess accelerometer and magnetometer data to produce quaternion input to the EKF. Formulation and simulation testing of a reduced-order implementation of the Gauss–Newton iteration method for this Kalman filter is documented in [19]. Preliminary experimental testing results are presented in [20].

In [21], Gallagher *et al.* present a nonoptimal complementary filter algorithm that has a lower computational complexity and similar accuracy to the work described by Bachmann *et al.* in [7] and [17]. Luinge describes a Kalman filter designed for human body tracking application in [22]–[24]. In the proposed method, inclination is determined without low-pass filtering accelerometer data. The design is based on assumptions concerning the frequency content of the acceleration and the magnitude of gravity. Reduction of drift about the vertical axis is dependent on the use of a kinematic human body model. Magnetometers are not used. More recently, Roetenberg *et al.* [25] extended the Kalman filter described in [23] to include a magnetometer model designed to prevent heading drift and compensate for magnetic disturbances. This compensation allowed a significant estimation accuracy improvement in comparison with no compensation or using angular rate sensors only. In [26], Zhu and Zhou describe a linear Kalman filter algorithm designed to smooth accelerometer and magnetometer readings from a nine-axis sensor module. Rather than estimating individual limb segment orientations relative to a fixed reference frame, as is done in this paper, their system determines joint angles in axis/angle form using the data from the two sensors mounted on the inboard and outboard sides of the joint. The axis/angle pairs are determined analytically using processed measurement data.

Kraft [27] describes an "unscented," quaternion-based Kalman filter for real-time estimation of rigid-body orientation using nine-axis sensor modules. The described filter approximates the Gaussian probability distribution using a set of sample points instead of linearizing nonlinear process model equations. Simulation results demonstrate the general validity of the described filter. Tests of the filter with real measurements are mentioned, but not shown or quantified. Haid and Breitenbach [28] also describe a Kalman filter algorithm for use with inertial and magnetic sensors. The primary aim of the filter is the elimination of drift and bias effects observed in low-cost angular rate sensors. The filter works only in the single dimension of the targeted angular-rate sensor. It does not estimate limb segment orientation or joint angles.

Some work has attempted to eliminate the need to include angular rate sensors in inertial/magnetic sensor modules. In [29], Gebre-Egziabher *et al.* describe an attitude determination algorithm for aircraft applications. The algorithm is based on a quaternion formulation of Wahba's problem [30], where magnetometer and accelerometer measurements are used to determine attitude without the use of angular rate sensors. A Kalman filter implementation of the algorithm is also presented. The algorithm is based on the assumption that the rigid body to which the sensor is attached is stationary or is slow moving, and is thus not applicable to highly dynamic tracking applications. Chin-Woo *et al.* [31] propose a gyroscope free inertial navigation system that uses accelerometers to determine both linear and angular motions of a rigid body. The approach requires a minimum of six accelerometers. Acceptable configurations and basic algorithms are examined through simulation. Use of accelerometers to calculate angular rate results in a faster orientation error growth rate than that associated with conventional angular rate sensors. This result is due to inclusion of the angular acceleration terms which introduce integrated noise and drift. The idea of using accelerometers to measure angular rate is carried further by Ang *et al.* in [32] and [33].

In contrast with the work described above, this paper presents a filter algorithm that is specifically designed for tracking human-limb segment orientation relative to an Earth-fixed frame. The algorithm incorporates a human body motion model. It adopts a two-layer filter architecture, in which the QUEST algorithm preprocesses accelerometer and magnetometer data and an EKF fuses the QUEST output with angular rate data.

III. MARG Sensors

Experimental data were collected using MARG III inertial/magnetic sensor modules designed by the authors and fabricated by McKinney Technology [8]. The MARG sensor design is based on its primary application, that is, human body motion tracking. Primary sensing components for this unit include Tokin CG-L43 ceramic rate gyros, Analog Devices ADXL202E micromachined accelerometers, and Honeywell HMC1051Z and HMC1052 one- and two-axis magnetometers. The sensor module also incorporates a Texas Instruments MSP430F149 ultra-low-power, 16-bit RISC architecture microcontroller. Overall, dimensions of the MARG III unit are approximately 1.8 cm$\times$3.0 cm$\times$2.5 cm.

The manufacturer specified maximum allowable angular rate of the CG-L43 ceramic gyro is $\pm$ 90°/s. This is deemed sufficient to quicken response in human body motion tracking applications, but not accurately measure rates associated with highly dynamic motion. Three of these gyros are orthogonally mounted

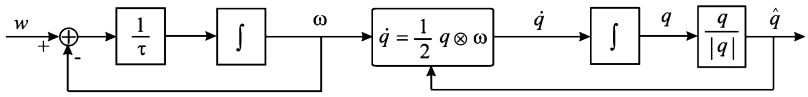

Fig. 1. Kalman filter process model. q is the orientation quaternion, ω is the angular velocity, w is a white noise, and τ is the time constant.

within the MARG unit to form a triad capable of measuring 3-DOF angular rate. In the results presented here, the limitations of the angular rate sensors did not affect the performance or demonstration of the algorithms during typical human motion.

The maximum measurement range of Analog Devices ADXL202E is $\pm$ 2 g, which is acceptable for sensing gravitational acceleration. The ADXL202E is a two-axis acceleration sensor on a single chip. As a result, only two of them are required to form a triad for measuring 3-DOF acceleration. The ADXL202E also offers a duty cycle output, which can be directly interfaced to a low-cost microcontroller without analog/digital (A/D) converters. The accelerometers are not used to measure linear accelerations associated with human motion.

In the MARG design, a one-axis HMC1051Z for the z-axis and a two-axis HMC1052 for x-y axes are mounted on the same PCB to form a three-axis magnetometer. The HMC1051Z and HMC1052 are specially designed to be mounted on the same PCB to form an orthogonal triad.

The purpose of the microcontroller is to convert analog sensor outputs to digital data, digitally filter the angular rate sensor data, and perform automatic set/reset of magnetometers to avoid magnetic saturation problems. To prepare angular rate data for processing by the Kalman filter, the data is averaged on start up to establish initial bias values. During run-time, angular rate data is preprocessed using a simple first-order high-pass filter to eliminate drift over time. Static bench tests have established that accelerometer and magnetometer data are relatively stable over time, and they are thus not bias-corrected at run-time. Magnetic interference is a major concern when using magnetometers in environments containing changing or distorted magnetic fields [34]. This is an active area of research by the authors and others [25]. No compensation for external magnetic effects is performed in the work described in this paper. It is noted that the MARG sensor is a prototype constructed using 2 g accelerometers and 90°/s angular rate sensors. These components were chosen for typical human motion, and may not be sufficient for extreme human motion. The algorithm presented in the paper is not limited to these particular sensor parameters.

IV. Kalman Filter Process Model

As stated above, the objective of this paper is to design a Kalman filter for real-time tracking of human body motion. To do so, it is necessary to establish a process model representing motion dynamics of the human musculoskeletal system. Dynamic models of the human musculoskeletal systems are complex, and have been studied for many years. Such models are ideal for computer simulations of articulated body motions, but remain too computationally demanding for real-time applications such as real-time human motion tracking. Thus, the challenge is to develop a model that is simple yet adequate for motion tracking applications. Based on extensive trial and error study, a first-order linear system model is adopted to represent the motion of each human body limb segment. Such a model is depicted in the left half of Fig. 1. It is assumed that each limb segment is independent of the others. The input to the linear system is a white noise w, and the output is the angular velocity ω of the limb segment. The most important parameter in this model is the time constant τ, which determines how fast a limb segment (e.g., upper arm) can move in typical human motion conditions. The angular velocity is thus modeled as a colored noise generated by a linear system with a white noise input.

In the filter, quaternions are used to represent the orientation of each body limb segment for two reasons. First, the quaternion representation does not suffer from the singularity problem associated with the Euler angle representation. Second, it avoids trigonometric functions in the filter algorithm, making it more efficient and easier to implement in real time on microcontrollers. In what follows, q will be used to denote the orientation quaternion in Earth coordinates. The angular velocity ω and the quaternion derivative $\dot{q}$ are related by the following well-known identity [35]:

$$\dot{q} = \frac{1}{2} q \otimes \omega \tag{1}$$

where $\otimes$ represents quaternion multiplication. Equation (1) is represented by the center block in Fig. 1. The quaternion derivative $\dot{q}$ is integrated to produce the quaternion q. In order to take advantage of computational simplifications and efficiencies associated with unit quaternions, the resultant quaternion is normalized to unit length in the last step of the process model, as shown in Fig. 1. The quaternion q produced by the integrator may not be exactly unit length, but it is normally very close to a unit quaternion. To avoid the complexity that the normalization introduces into the Kalman filter derivation, it is not included in the process model equations presented in the next section. As a result, although the Kalman filter is an optimal algorithm, this normalization procedure leads to a suboptimal algorithm. In the next section, two Kalman filter designs based on this process model will be presented.

V. Kalman Filter Design

Two alternative approaches to the Kalman filter design based on the process model presented in Section IV will be described in this section. The state vector for both approaches is the same. It is a 7-D vector consisting of the three components of angular rate and the four elements of the orientation quaternion. The difference between the two approaches is in the measurement or output equation for the Kalman filter. The first approach uses a standard Kalman filter design, which has a 9-D measurement vector, consisting of 3-D angular rate, 3-D acceleration, and 3-D local magnetic field. This 9-D vector directly corresponds to the measurements provided by inertial/magnetic sensors modules. The first three components of the output equation (angular rate portion) are linearly related to the state vector. However, the

other six components of the output equation are nonlinearly related to the state vector. The nonlinear relationship is quite complicated. As a result, the EKF designed with this output equation is computationally inefficient.

The second approach uses a separate algorithm to find a corresponding quaternion for each set of accelerometer and magnetometer measurements. The computed quaternion is then combined with the angular rate measurements, and presented to the Kalman filter as its measurements. By doing so, the output equations for the Kalman filter become linear, and the overall Kalman filter design is greatly simplified.

A. The First Approach

The first approach is a standard Kalman filter design based on the process model depicted in Fig. 1. The state vector x is 7-D, with the first three components being the angular rate ω, and the last four components being the quaternion q. That is

$$\begin{bmatrix} x_1 \\ x_2 \\ x_3 \end{bmatrix} = \begin{bmatrix} \omega_1 \\ \omega_2 \\ \omega_3 \end{bmatrix} = \omega, \quad \begin{bmatrix} x_4 \\ x_5 \\ x_6 \\ x_7 \end{bmatrix} = \begin{bmatrix} q_1 \\ q_2 \\ q_3 \\ q_4 \end{bmatrix} = q.$$

Based on Fig. 1, the state equations are given by

$$\begin{bmatrix} \dot{x}_1 \\ \dot{x}_2 \\ \dot{x}_3 \end{bmatrix} = \frac{1}{\tau}\left(- \begin{bmatrix} x_1 \\ x_2 \\ x_3 \end{bmatrix} + \begin{bmatrix} w_1 \\ w_2 \\ w_3 \end{bmatrix} \right) \tag{2}$$

$$\begin{bmatrix} \dot{x}_4 \\ \dot{x}_5 \\ \dot{x}_6 \\ \dot{x}_7 \end{bmatrix} = \frac{1}{2} \begin{bmatrix} x_4 \\ x_5 \\ x_6 \\ x_7 \end{bmatrix} \otimes \begin{bmatrix} 0 \\ x_1 \\ x_2 \\ x_3 \end{bmatrix}. \tag{3}$$

It is noted that quaternion normalization is not modeled in these state equations, but is carried out in the real-time implementation.

Since measurement data to the filter are provided by MARG sensors, it is natural to choose the following as the measurements of the Kalman filter:

$$\begin{bmatrix} z_1 \\ z_2 \\ z_3 \end{bmatrix} = \begin{bmatrix} x \text{ component of angular rate} \\ y \text{ component of angular rate} \\ z \text{ component of angular rate} \end{bmatrix}$$

$$\begin{bmatrix} z_4 \\ z_5 \\ z_6 \end{bmatrix} = \begin{bmatrix} x \text{ component of acceleration} \\ y \text{ component of acceleration} \\ z \text{ component of acceleration} \end{bmatrix}$$

$$\begin{bmatrix} z_7 \\ z_8 \\ z_9 \end{bmatrix} = \begin{bmatrix} x \text{ component of local magnetic field} \\ y \text{ component of local magnetic field} \\ z \text{ component of local magnetic field} \end{bmatrix}.$$

Since angular rates are part of the state, the first three measurement equations are simply given by the following:

$$z_1 = x_1 + v_1 \tag{4}$$

$$z_2 = x_2 + v_2 \tag{5}$$

$$z_3 = x_3 + v_3 \tag{6}$$

where v_i is the measurement noise that is assumed to be white. As for the remaining six measurement equations, they turn out to be quite complicated. As an example, the seventh measurement equation is given by

$$z_7 = \left(\left(x_4^2 + x_7^2 - x_5^2 - x_6^2\right)/h_1 + 2(x_4x_5 - x_6x_7)/h_2 + 2(x_4x_6 + x_5x_7)/h_3\right) / \left(x_4^2 + x_5^2 + x_6^2x_7^2\right) + v_4 \tag{7}$$

where h_1, h_2, and h_3 are values of the Earth magnetic field measured in the Earth coordinates, which are constant for a given location. It is not difficult to design an EKF, as shown in Fig. 2, based on state (2) and (3), and the nine measurement equations, which was indeed carried out in [36]. The problem is that computational requirements for implementing such a filter are extremely high, making it unfeasible for real-time motion tracking. An alternative approach to the Kalman filter design is thus presented in the next subsection.

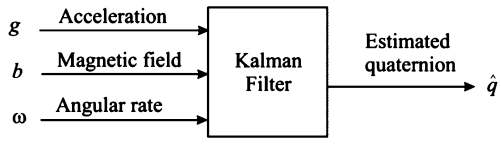

Fig. 2. Block diagram of the first approach to Kalman filter design.

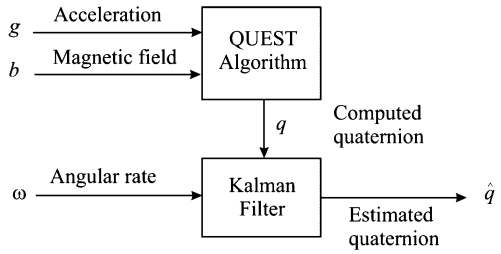

Fig. 3. Block diagram of the second approach to Kalman filter design.

B. The Second Approach

Fig. 3 shows a block diagram of an alternative approach to filter design. Acceleration and local magnetic field measurements are used as input to the QUEST algorithm [37] to produce what will be called *the computed quaternion*. The computed quaternion together with angular rate measurements is then presented to a Kalman filter as measurements. It will be seen below that the Kalman filter in this case is significantly simpler, owing to the fact that the measurement equations are linear. It is true that there is an additional computational cost to implement the QUEST algorithm in this approach. Still, the overall computational requirements for this approach are much less than what is needed for the first approach.

The QUEST (quaternion estimator) algorithm is a popular algorithm for a single-frame estimation of an attitude quaternion [37]. The algorithm was created to solve Wahba's problem [30] that involved determination of the attitude of a rigid body in reference to a fixed coordinate system based on a set of measurement or observation vectors using a closed form solution. The minimum number of measurement vectors required to compute orientation is two. Early solutions to Wahba's problem directly compute a rotation matrix capable of rotating the measurement (assuming no errors) vectors to match the reference vectors. The

QUEST algorithm solves Wahba's problem by calculating the four elements of the corresponding optimal quaternion [37].

This alternative approach to filter design as shown in Fig. 3 is not without reasons. If the limb segment to which an inertial/magnetic sensor module is attached is stationary, acceleration (gravity) and local magnetic field measurements are sufficient to determine the orientation of the body. While stationary, accelerometers measure the local gravity vector in the body frame. The 3-D gravity measurements can be used to determine roll and pitch angles of the body relative to the fixed Earth frame. The yaw angle of the body is determined from the local magnetic field measurements. In this application, the QUEST algorithm takes gravity and magnetic field measurement vectors with equal weight and computes the optimal quaternion that will rotate these vectors to match their corresponding reference vectors.

While the rigid body is in motion, the computed quaternions from this algorithm do not represent the actual real-time orientation of the body, because accelerometers measure the sum of gravity and motion induced acceleration. This is where angular rate measurements come to help estimate the orientation of the rigid body. While angular rate measurements can be integrated to yield an orientation estimate, they are prone to drift over an extended period of time. Acceleration and magnetic field measurements do not drift over time. The Kalman filter in this approach is designed to optimally fuse the complementary information provided by the angular rate measurements and the computed quaternion.

It should be pointed out that this filtering architecture has been previously proposed and successfully applied in other areas such as attitude heading and reference systems (AHRS) [38]. In [38], an inertial navigation system for autonomous underwater vehicles was developed, in which a complementary filter first combines measurement data from accelerometers, angular rate sensors, and magnetic sensors. An EKF then fuses the output of the complementary filter with the GPS/DGPS measurements.

The state equations in the second approach are the same as those in the first approach, that is, equations (2) and (3). The measurement equations in this case are much simpler, and they are

$$z_i = x_i + v_i, \quad i = 1, \ldots, 7 \tag{8}$$

where v_i is the white noise measurement. Although the measurement equations are linear, an EKF is still required since the second part of the state (3) is nonlinear. Nevertheless, linearity in the measurement equations significantly simplifies the filter design and reduces computational requirements for real-time implementation.

C. Discussion

The first-order process model and an early version of the second approach to the Kalman filter design was first reported in [18]. Rather than using the QUEST algorithm, a Gauss–Newton iteration method was used to preprocess accelerometer and magnetometer data to produce quaternion input to the EKF. A reduced-order implementation of the Gauss–Newton iteration method was described in [19]. This reduced order implementation requires computing the inverse of a 3×3 matrix rather than that of a 4×4 matrix. The Gauss–Newton iteration method was replaced by the factored quaternion algorithm in [20]. While more efficient, the factored quaternion algorithm provides a suboptimal solution. The QUEST algorithm provides an optimal solution for noisy measurement data. Preliminary experimental results were also reported in [20]. In this paper, the QUEST algorithm is adopted to preprocess the acceleration and magnetic field measurement data. The QUEST algorithm requires computing the inverse of a 4×4 matrix, but it is a single-frame or noniterative algorithm. The QUEST algorithm needs to be executed once for each sampling step of the Kalman filter. The Gauss–Newton method needs to be iteratively evaluated several times until it converges for each sampling step of the Kalman filter.

VI. Kalman Filter Implementation

In this section, the implementation of the second approach Kalman filter design will be described. First, the state equations are linearized and discretized to yield a discrete process model. Second, modeling of the process noises and measurement noises is presented.

The state equations (2) and (3) can be written together in the following form:

$$\dot{x} = f(x) + w(t). \tag{9}$$

This nonlinear process model can be linearized along the currently estimated trajectory $\hat{x}$

$$\Delta\dot{x} = \frac{\partial f(x)}{\partial x}\Big|_{x=\hat{x}} \Delta x + w(t). \tag{10}$$

The actual trajectory x is the sum of the estimated trajectory $\hat{x}$ and the small increment Δx

$$x = \hat{x} + \Delta x. \tag{11}$$

The next step is to convert the continuous-time model (10) into a discrete-time model. Let $\delta = \Delta t$ be the sampling interval. Then the difference equation corresponding to the differential (10) is given by

$$\Delta x_{k+1} = \Phi_k \Delta x_k + w_k \tag{12}$$

where the discrete state transition matrix is

$$\Phi_k = \begin{bmatrix} e^{-\frac{\delta}{\tau_1}} & 0 & 0 & 0 & 0 & 0 & 0 \\ 0 & e^{-\frac{\delta}{\tau_2}} & 0 & 0 & 0 & 0 & 0 \\ 0 & 0 & e^{-\frac{\delta}{\tau_3}} & 0 & 0 & 0 & 0 \\ -\frac{\hat{x}_5\delta}{2} & -\frac{\hat{x}_6\delta}{2} & -\frac{\hat{x}_7\delta}{2} & 1 & -\frac{\hat{x}_1\delta}{2} & -\frac{\hat{x}_2\delta}{2} & -\frac{\hat{x}_3\delta}{2} \\ \frac{\hat{x}_4\delta}{2} & -\frac{\hat{x}_7\delta}{2} & \frac{\hat{x}_6\delta}{2} & \frac{\hat{x}_1\delta}{2} & 1 & \frac{\hat{x}_3\delta}{2} & -\frac{\hat{x}_2\delta}{2} \\ \frac{\hat{x}_7\delta}{2} & \frac{\hat{x}_4\delta}{2} & -\frac{\hat{x}_5\delta}{2} & \frac{\hat{x}_2\delta}{2} & -\frac{\hat{x}_3\delta}{2} & 1 & \frac{\hat{x}_1\delta}{2} \\ -\frac{\hat{x}_6\delta}{2} & \frac{\hat{x}_5\delta}{2} & \frac{\hat{x}_4\delta}{2} & \frac{\hat{x}_3\delta}{2} & \frac{\hat{x}_2\delta}{2} & -\frac{\hat{x}_1\delta}{2} & 1 \end{bmatrix} \tag{13}$$

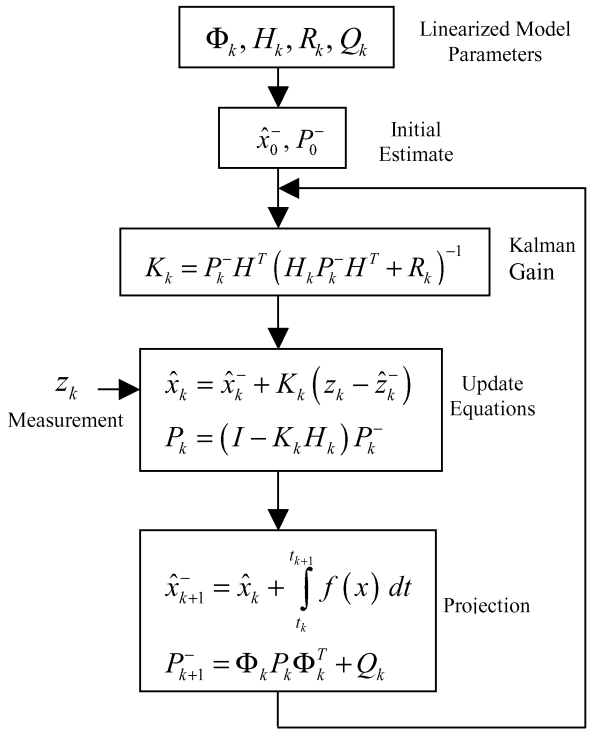

Fig. 4. Block diagram of the EKF.

and w_k is a vector of discrete white process noise and its elements are given by

$$w_{ik} = \begin{cases} \int_{t_k}^{t_{k+1}} e^{-\frac{t_{k+1}-\gamma}{\tau_i}} w_i(\gamma) d\gamma, & i = 1,2,3 \\ 0, & i = 4,5,6,7. \end{cases} \tag{14}$$

The measurement (8) are linear and thus linearization is not required. The corresponding discrete measurement equation is given by

$$z_k = H_k x_k + v_k \tag{15}$$

where H_k is the 7×7 identity matrix. An EKF can now be designed for the discrete process (12) and the discrete measurement (15). A complete diagram of the filter is depicted in Fig. 4. It is seen from Fig. 4 that the model parameters Φ_k, H_k, R_k, and Q_k need to be provided to start the filter. Φ_k is the discrete state transition matrix given by (13). H_k is the identity measurement equation matrix of (15). The determination of the covariance matrix Q_k of the process noises and the covariance matrix R_k of the measurement noises is discussed below.

The process noise covariance matrix Q_k is defined by

$$Q_k = E[w_k w_k^T] \tag{16}$$

where E is the expectation operator, and w_k is the discrete process white noise vector of (12), whose components are given by (14). Before computing Q_k, it should be noted that the continuous process noises $w(t) = [w_1(t), w_2(t), w_3(t)]^T$ of the state (2) are independent white noises with zero mean and variance D_i. As such, the covariance is given by

$$E[w_i(t) w_j(s)] = \begin{cases} D_i \delta(t-s), & i = j \\ 0, & i \neq j. \end{cases} \tag{17}$$

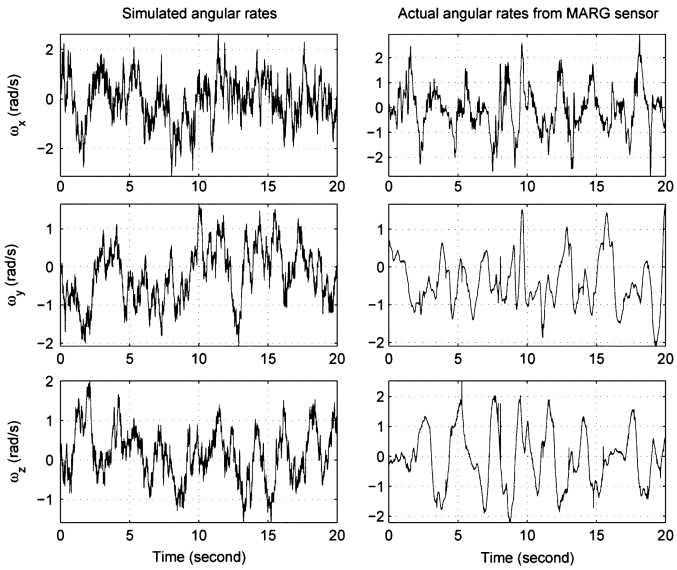

Fig. 5. Comparison of the simulated angular rate (left) and actual angular rate measurements (right).

Using (17) and (14), the process noise covariance matrix Q_k of (16) is evaluated to be

$$Q_k = \begin{bmatrix} q_{11} & 0 & 0 & 0 & 0 & 0 & 0 \\ 0 & q_{22} & 0 & 0 & 0 & 0 & 0 \\ 0 & 0 & q_{33} & 0 & 0 & 0 & 0 \\ 0 & 0 & 0 & 0 & 0 & 0 & 0 \\ 0 & 0 & 0 & 0 & 0 & 0 & 0 \\ 0 & 0 & 0 & 0 & 0 & 0 & 0 \\ 0 & 0 & 0 & 0 & 0 & 0 & 0 \end{bmatrix} \tag{18}$$

where q_{11}, q_{22}, and q_{33} are given by

$$q_{11} = E[w_{1k} w_{1k}] = \frac{D_1}{2\tau_1}\left(1 - e^{-\frac{2\Delta t}{\tau_1}}\right) \tag{19}$$

$$q_{22} = E[w_{2k} w_{2k}] = \frac{D_2}{2\tau_2}\left(1 - e^{-\frac{2\Delta t}{\tau_2}}\right) \tag{20}$$

$$q_{33} = E[w_{3k} w_{3k}] = \frac{D_3}{2\tau_3}\left(1 - e^{-\frac{2\Delta t}{\tau_3}}\right). \tag{21}$$

What remains to be determined are the variance D_i of the continuous white noise processes and the time constant τ_i of the process model. They are determined using actual measurement data from the MARG sensors and a Matlab simulation implementing the angular rate process model (2). The variance and time constant in the simulation are adjusted until the output of the simulation closely matches the actual measurement data. For this purpose, a MARG sensor was attached to the right lower arm of a user and typical arm motion data were collected. It was experimentally determined that $\tau_i = 0.5$ s, $D_i = 0.4$ rad^2/s^2.

Fig. 5 shows a comparison between the simulated angular rates and the actual angular rates obtained from a MARG III sensor for typical arm motions. The graphs to the left represent the angular rates generated by the simulation model. The graphs to the right are the angular rates measured by a MARG sensor. It can be observed that the two sets of data exhibit similar characteristics. Autocorrelations of the simulated and actual x-axis angular rate data are plotted in Fig. 6. The autocorrelation of the actual angular rate data obtained from the MARG sensor was

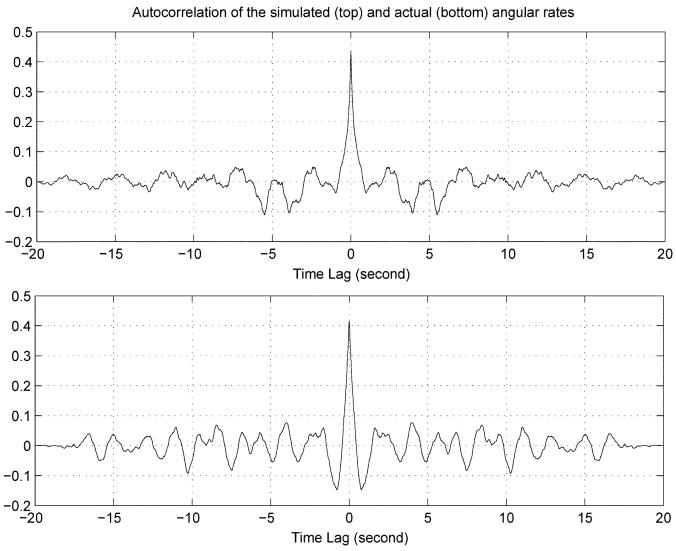

Fig. 6. Autocorrelations of the simulated x-axis angular rate (top plot) and the actual x-axis angular rate (bottom plot).

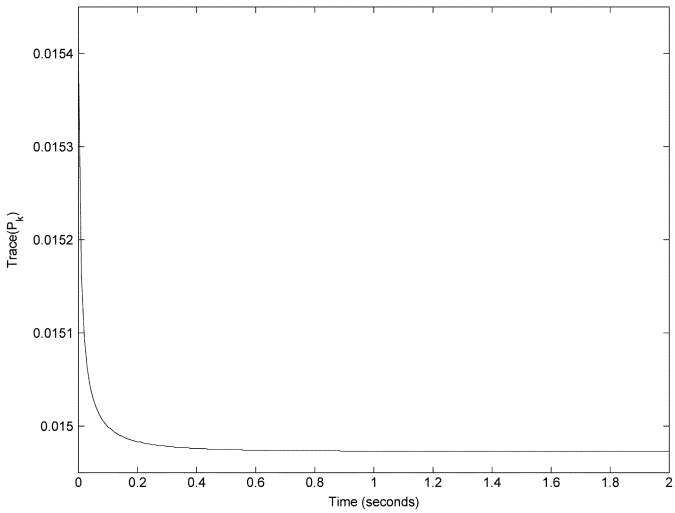

Fig. 7. Trace of the error covariance matrix.

first computed. The parameters of the process model were then adjusted so that the autocorrelation of the simulated angular rate closely matches that of the actual data. It is seen that they are not exactly the same, but closely resemble each other.

The measurement noise covariance matrix R_k represents the level of confidence placed in the accuracy of the measurements, and is given by

$$R_k = E[v_k v_k^T]. \tag{22}$$

In principle, R_k is not necessarily diagonal. For practical purposes, only diagonal elements are experimentally determined based on actual measurements. A MARG sensor was placed in various static configurations, and data were collected. The variances of the first three measurement components are determined directly from angular rate measurements, and the variances of the other four components (quaternion components) are determined using computed quaternions. The experimentally determined values are $R_{11} = R_{22} = R_{33} = 0.01$ rad^2/s^{-2}, and $R_{44} = R_{55} = R_{66} = R_{77} = 0.0001$.

VII. Offline MATLAB Testing Results

After deriving all the required parameters to initialize the Kalman filter, it was implemented using MATLAB to test the performance and accuracy of the quaternion orientation estimates. Real world data recorded using a MARG sensor was used in these tests.

Since the Kalman gain was determined such that the sum of squared errors is minimized, one way to measure the convergence of the Kalman filter is through examination of the trace of the error covariance matrix P_k. Fig. 7 shows the trace of P_k for the first 200 samples of data obtained with the sensor in its reference position (x-axis pointing north, y-axis pointing east, and z-axis point down). It is noted that the sum of squared errors reaches a steady state after approximately 0.6 s.

Table I shows the elements of the quaternion for the first five samples. The initial estimate was chosen to be the unit quaternion (0.5, 0.5, 0.5, 0.5). The actual position of the sensor in the reference position is represented by the quaternion (1, 0, 0, 0). The data shown in Table I indicates that the Kalman filter estimate converged to the actual position in a single iteration.

TABLE I
Convergence of the Quaternion Estimates

Sample	$\hat{q}_0$	$\hat{q}_1$	$\hat{q}_2$	$\hat{q}_3$
1	0.99985	0.0082135	0.0066032	0.013570
2	0.99991	0.0057585	0.0049037	0.011901
3	0.99990	0.0055983	0.0048826	0.011882
4	0.99990	0.005288	0.0046884	0.011784
5	0.99990	0.0052297	0.0046353	0.011506

While the QUEST algorithm works well for static orientation and slow movements, the objective of the Kalman filter is to blend angular rate measurements with the estimates produced using magnetometer and accelerometer data during periods in which the sensor module is subjected to motions involving high angular rates and large linear accelerations. To verify the estimation accuracy during such periods, the orientation estimates of the Kalman filter were compared with the estimates produced using only the QUEST algorithm with no rate measurement and with the reference motion of a precision tilt table. Two kinds of experiments were conducted for this test. The first used controlled rotations produced by a HAAS precision tilt table. The table has two DOFs and is capable of positioning to an accuracy of 0.001° at rates ranging from 0.001 to 80°/s. In order to mitigate any possible magnetic effects generated by the steel construction of the tilt table, the sensor package was mounted on a nonferrous extension above the table as shown in Fig. 8. The extension is made of a piece of PVC pipe and is approximately 1 m in length. The second experiment used a random motion pattern produced while the sensor was attached to the arm of a person.

In the first set of experiments, the sensor was initially placed with its xyz axes aligned with north-east-down directions. The sensor was rotated $-90°$ about the x-axis at a rate of 60°/s and then rotated 90° at the same rate (in the reverse direction) for

Fig. 8. Experimental setup using a HAAS precision tilt table.

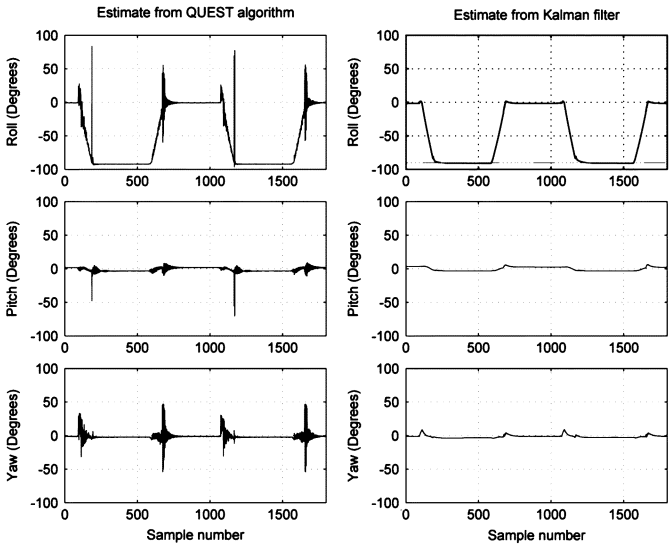

Fig. 9. Orientation estimate produced by the QUEST algorithm (left) and the Kalman filter (right) with a 90° rotation in roll axis.

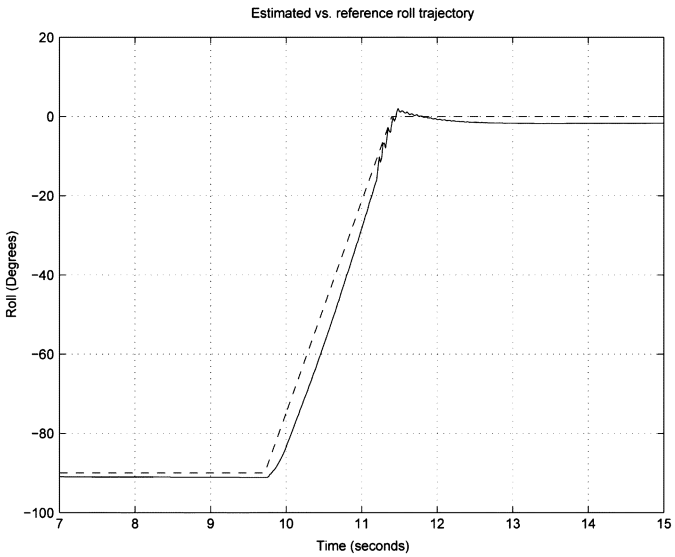

Fig. 10. Zoom-in view of the roll estimate (solid curve) from the Kalman filter and the tilt table reference motion (dashed curve) with a 90° rotation in roll.

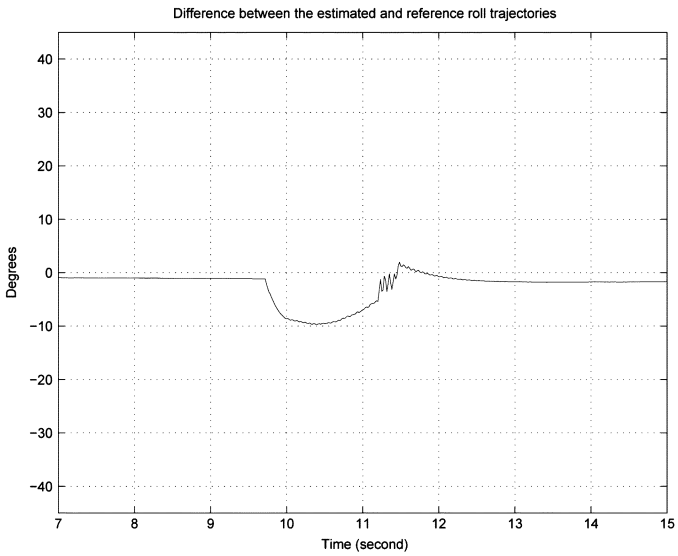

Fig. 11. Difference between the roll estimate and the tilt table reference motion.

two cycles. Fig. 9 shows the performance of the Kalman filter in estimating the orientation of the sensor. The graphs to the left show the orientation estimated by the QUEST algorithm, and the graphs to the right show the orientation estimated by the Kalman filter. It can be seen that the QUEST algorithm was able to correctly estimate the roll angle before the first (negative) rotation, between the first and second (positive) rotations, and after the second rotation, but it is not able to correctly estimate orientation during the rotational motions. During the rotational motions, the accelerometers measure the sum of gravity and motion induced acceleration. Without rate sensors, the QUEST algorithm is not able to differentiate gravity from the motion acceleration. Relatively large errors in pitch and yaw were also produced by the QUEST algorithm. On the other hand, it can be seen from the top-right plot that the Kalman filter was able to correctly estimate the roll angle throughout the duration of the experiment. The small pitch and yaw motions seen in the center-right and bottom-right plots are due to misalignment of the sensor module with the motion axes of the experimental tilt table. The misalignments were corrected manually, but could not be completely removed without the use of equipment not available to the authors. To confirm that the errors were due to misalignments, the algorithm was tested using synthetically generated, noise-free data with rotation in only one axis. These results demonstrated that the algorithm does not produce any observable cross-coupling responses in other axes.

To illustrate the accuracy of the Kalman filter, the estimates produced by the Kalman filter can be compared with the motion of the tilt table. Since the tilt table used in the experiments is much more accurate than the tracking system under evaluation, its motion can be treated as a truth reference. In Fig. 10, the top-right plot of Fig. 9 is replotted in a zoom-in view for the time period of 7–15 s. The solid curve represents the roll estimate from the Kalman filter, and the dashed curve is the reference trajectory of the tilt table. The difference between these two curves is shown in Fig. 11. It is observed from Figs. 10 and 11 that the static accuracy of the filter is better than 2° for the time

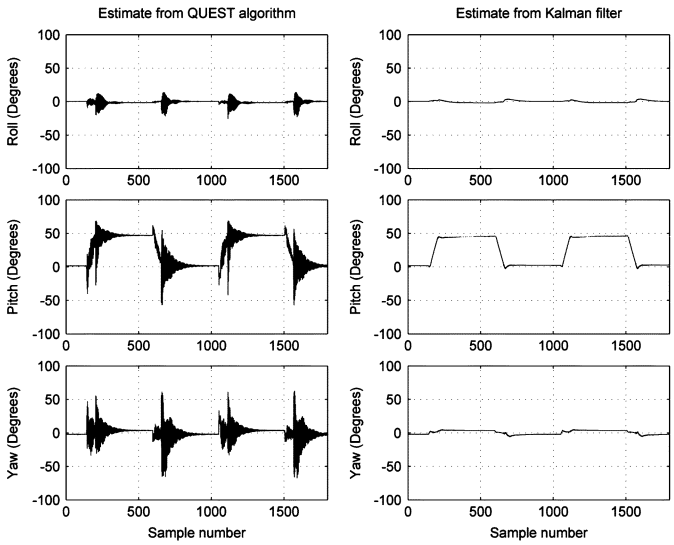

Fig. 12. Orientation estimate produced by the QUEST algorithm (left) and the Kalman filter (right) with a 45° rotation in pitch axis.

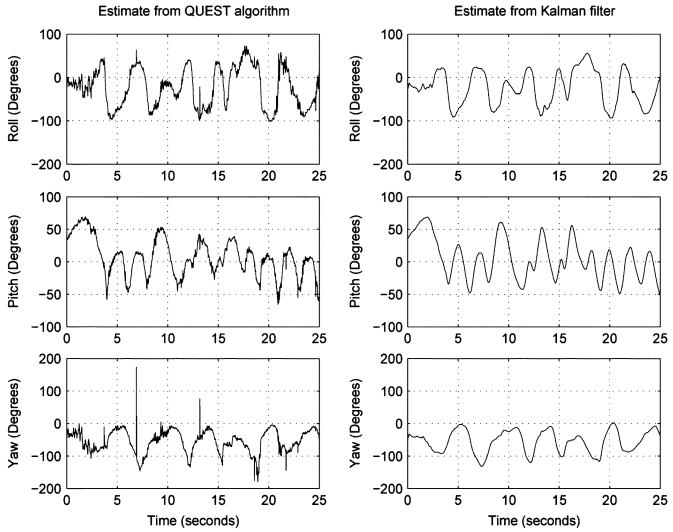

Fig. 13. Orientation estimate produced by the QUEST algorithm (left) and the Kalman filter (right) with random arm movements.

Fig. 14. Snapshot of real-time testing. The user with two MARG sensors attached to the right arm is the foreground and the human avatar projected on a screen is in background.

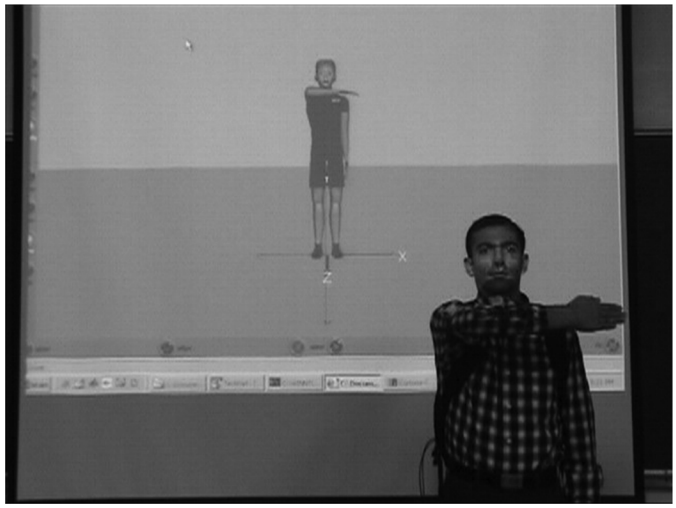

Fig. 15. Another snapshot of real-time testing.

periods of about 7–9.8 s and 11.3–15 s. During the time period of 9.8–11.3 s, the tilt table and the MARG sensor are in the dynamic state moving from -90.0° to 0.0° at the rate of 60°/s. It can be observed from Fig. 11 that the maximum error is about 9°. This large dynamic error is mainly due to the lag of the tracking system. The lag is on the order of 100 ms, as depicted by the horizontal gap between the blue curve and green curve during the time period of 10–11 s. The sampling rate is 100 Hz, which yields a lag of 10 ms. The computational time required to execute the filter algorithm is about 1.6 ms. The additional lag is caused by data transmission. In human body tracking applications, this lag-induced error is only observable during highly dynamic motion, and is not of great enough magnitude to impair user interaction with a virtual environment.

Fig. 12 shows plots of rotating the sensor about the y-axis first by 45° and then by -45° at a rate of 45°/s. Similar results are observed in this experiment.

Fig. 13 shows the results of an experiment in which the sensor was rotated randomly while attached to the arm of a person. Although there is no true reference in this case, it can be seen that the Kalman filter eliminated the jittering and spiking contained in the orientation estimates produced by using the QUEST algorithm alone.

VIII. Real-Time Testing Results

After initial testing of the EKF with the MATLAB implementation, the QUEST algorithm and EKF algorithm were implemented in Java for real-time testing and evaluation. Computation time required to perform a single update is 1.6 ms. Memory management in the Java implementation is carefully performed to avoid the requirement for garbage collection and possible interruption of filter processing. The real-time quaternion produced by the Kalman filter was visualized using a human-like avatar as seen in Figs. 14 and 15. Two MARG sensors were used to track the motion of a human arm, one sensor being attached to the upper arm and the other attached to the lower arm. A video clip demonstrating real-tracking of human arm motions is available at http://ieeexplore.ieee.org.

The QUEST algorithm was able to track the motion of the human arm under slow-moving conditions where linear acceleration was not significant. However, when the arm motion became faster, the algorithm was not able to follow the arm motion, resulting in observable lag as well as overshoots.

When the EKF was integrated with the QUEST algorithm, the avatar was able to successfully track the human arm motion in real time under all conditions. Furthermore, the filtering process did not produce any noticeable lag. Movement of the human arm and the avatar was synchronized.

IX. Conclusion

This paper presents the design, implementation, and experimental results of a quaternion-based Kalman filter for real-time human body motion tracking using inertial/magnetic sensor modules containing orthogonally mounted triads of accelerometers, angular rate sensors, and magnetometers. This subject filter is not applicable to applications in which accelerations due to forces other than gravity are present for indefinite periods. The filter was designed with the goal of being able to produce highly accurate orientation estimates in real time. This real-time requirement precluded the use of complex models of human motion. Instead the filter design makes use of a simple first-order linear system model. Output of the model is angular velocity modeled as colored noise generated from white noise input. The Kalman filter design is further simplified by preprocessing accelerometer and magnetometer data using the single-frame QUEST algorithm. The quaternion produced by QUEST is provided as input to the Kalman filter along with angular rate data. In comparison to more traditional approaches, this preprocessing step significantly reduces the complexity of filter design by allowing the use of linear measurement equations. Prior to testing of the filter algorithm, values for variances and time constants where determined by comparing simulation results to actual measurement data obtained during typical arm motions. This process was considered complete when the autocorrelation of the simulation data closely matched that of the actual data. In experiments designed to validate filter performance, this approach was shown to work well. In these experiments, filter orientation estimates were compared with truth data obtained from a rotary tilt table. Filter response very closely matched tilt table motion with a static accuracy better than 2° and a dynamic accuracy of better than 9°. This larger error during motion was largely caused by data communication delays. Even with this delay, qualitative experiments in which the algorithm was used demonstrate that these dynamic errors were not of great enough magnitude to impair user interaction with a virtual environment.

The Kalman filter design presented in this paper is the result of several years of effort. With refinement of this design and others mentioned in the related work section, orientation estimation algorithms have reached a limit given the accuracy and noise characteristics of the MEMs sensors employed in the application. The angular rate sensors and accelerometers are truly "sourceless" and do not depend on any outside reference. However, though it is not artificially generated, the magnetometers must sense a homogenous ambient magnetic field in order for these systems to deliver orientation estimates that are stable in azimuth. Thus the ultimate accuracy of these algorithms can not be determined by considering only the sensors and the implemented algorithms.

Acknowledgment

The authors would like to thank Dr. R. McGhee for insightful advice and guidance throughout this project, J. Calusdian for technical support, C. Aparicio for implementing the Kalman filter and conducting experimental testing, and D. McKinney for collaboration on the MARG sensors.

References

[1] Gypsy4 Mechanical Motion Capture 2004 [Online]. Available: http://www.animazoo.com/products/gypsy4.htm.

[2] Products: Phantom 1.5/6DOF and 3.0/6DOF 2005 [Online]. Available: http://www.sensable.com/products/phantom_ghost/premium6DOF.asp

[3] G. Welch, G. Bishop, L. Vicci, S. Brumback, K. Keller, and D. Colucci, "The HiBall tracker: High-performance wide-area tracking for virtual and augmented environments," in *Proc. ACM Symp. Virtual Reality Softw. Technol.*, London, U.K., Dec. 1999, pp. 1–11.

[4] Motion Capture Systems From Vicon Peak 2005 [Online]. Available: http://www.vicon.com/

[5] Qualisys Motion Cature Analysis System of Kinematics Data 2005 [Online]. Available: http://www.qualisys.com/

[6] F. Raab, E. Blood, O. Steiner, and H. Jones, "Magnetic position and orientation tracking system," *IEEE Trans. Aerosp. Electron. Syst.*, vol. AES-15, no. 5, pp. 709–717, May 1977.

[7] E. R. Bachmann, R. B. McGhee, X. Yun, and M. J. Zyda, "Inertial and magnetic posture tracking for inserting humans into networked virtual environments," in *Proc. ACM Symp. Virtual Reality Softw. Technol.*, Banff, AB, Canada, Nov. 2001, pp. 9–16.

[8] E. R. Bachmann, X. Yun, D. McKinney, R. B. McGhee, and M. J. Zyda, "Design and implementation of MARG sensors for 3-DOF orientation measurement of rigid bodies," in *Proc. IEEE Int. Conf. Robot. Autom.*, Taipei, Taiwan, May 2003, vol. 1, pp. 1171–1178.

[9] J. Lee and I. Ha, "Sensor fusion and calibration for motion captures using accelerometers," in *Proc. IEEE Int. Conf. Robot. Autom.*, Detroit, MI, May 1999, pp. 1954–1959.

[10] H. Rehbinder and X. Hu, "Drift-free attitude estimation for accelerated rigid bodies," in *Proc. IEEE Int. Conf. Robot. Autom.*, Seoul, Korea, May 2001, pp. 4244–4249.

[11] A. M. Sabatini, C. Martelloni, S. Scapellato, and F. Cavallo, "Assessment of walking features from foot inertial sensing," *IEEE Trans. Aerosp. Electron. Syst.*, vol. 52, no. 3, pp. 486–494, Mar. 2005.

[12] A. M. Sabatini, "Quaternion-based strap-down integration method for applications of inertial sensing to gait analysis," *Med. Biol. Eng. Comput.*, vol. 43, no. 1, pp. 94–101, Jan. 2005.

[13] P. H. Veltink, P. Slycke, J. Hemssems, T. Buschman, G. Bulstra, and H. Hermens, "Three dimensional inertial sensing of foot movements for automatic tuning of a two-channel implantable drop-foot stimulator," *Med. Eng. Phys.*, vol. 25, no. 1, pp. 21–28, Jan. 2003.

[14] R. Azuma and G. Bishop, "Improving static and dynamic registration in an optical see-through HMD," in *Proc. 21st Annu. Conf. Comput. Graph. Interactive Techniques*, Orlando, FL, Jul. 1994, pp. 197–204.

[15] E. Foxlin, M. Harrington, and Y. Alshuler, "Miniature 6DOF inertial for track HMDs," in *Proc. SPIE Helmet, Head-Mounted Displays III,*, Orlando, FL, Apr. 1998, vol. 3362, pp. 214–228.

[16] E. Foxlin, "Inertial head-tracker fusion by a complementary separate-bias Kalman filter," in *Proc. Virtual Reality Annu. Int. Symp.*, Santa Clara, CA, Mar. 1996, pp. 185–194.

[17] E. R. Bachmann, "Inertial and magnetic tracking of limb segment orientation for inserting humans into synthetic environments," Ph.D. dissertation, Naval Postgraduate School, Monterey, CA, 2000.

[18] J. L. Marins, X. Yun, E. R. Bachmann, R. B. McGhee, and M. J. Zyda, "An extended Kalman filter for quaternion-based orientation estimation using MARG sensors," in *Proc. IEEE/RSJ Int. Conf. Intell. Robots Syst.*, Maui, HI, Oct. 2001, pp. 2003–2011.

[19] X. Yun, M. Lizarraga, E. Bachmann, and R. McGhee, "An improved quaternion-based kalman filter for real-time tracking of rigid body orientation," in *Proc. IEEE/RSJ Int. Conf. Intell. Robots Syst.*, Las Vegas, NV, Oct. 2003, vol. 2, pp. 27–31.

[20] X. Yun, C. Aparicio, E. R. Bachmann, and R. B. McGhee, "Implementation and experimental results of a quaternion-based Kalman filter for human body motion tracking," in *Proc. IEEE Int. Conf. Robot. Autom.*, Barcelona, Spain, Apr. 2005, pp. 317–322.
[21] A. Gallagher, Y. Matsuoka, and W.-T. Ang, "An efficient real-time human posture tracking algorithm using low-cost inertial and magnetic sensors," in *Proc. IEEE Int. Conf. Robot. Autom.*, Sendai, Japan, Sep. 28–Oct. 2, 2004, pp. 2967–2972.
[22] H. J. Luinge, P. H. Veltink, and C. T. Baten, "Estimating orientation with gyroscopes and accelerometers," *Technol. Health Care*, vol. 7, no. 6, pp. 455–459, Jan. 1999.
[23] H. J. Luinge, "Inertial sensing of human movement," Ph.D. dissertation, Univ. Twente, Enschede, The Netherlands, Dec. 2002.
[24] H. J. Luinge and P. H. Veltink, "Inclination measurement of human movement using a 3-D accelerometer with autocalibration," *IEEE Trans. Neural Syst. Rehab. Eng.*, vol. 12, no. 1, pp. 112–121, Mar. 2004.
[25] D. Roetenberg, H. J. Luinge, T. M. Baten, and P. H. Veltink, "Compensation of magnetic disturbances improves inertial and magnetic sensing of human body segment orientation," *IEEE Trans. Neural Syst. Rehab. Eng.*, vol. 13, no. 3, pp. 395–405, Sep. 2005.
[26] R. Zhu and Z. Zhou, "A real-time articulated human motion tracking using tri-axis inertial/magnetic sensors package," *IEEE Trans. Neural Syst. Rehab. Eng.*, vol. 12, no. 2, pp. 295–302, Jun. 2004.
[27] E. Kraft, "A quaternion-based unscented Kalman filter for orientation tracking," in *Proc. IEEE 6th Int. Conf. Inf. Fusion*, Cairns, Queensland, Australia, 2003, pp. 47–54.
[28] M. Haid and J. Breitenbach, "Low cost inertial orientation tracking with Kalman filter," *Appl. Math. Comput.*, vol. 153, pp. 567–575, 2004.
[29] D. Gebre-Egziabher, G. H. Klkaim, J. Powell, and B. W. Parkinson, "A gyro-free quaternion-based attitude determination system suitable for implementation using low cost sensors," in *Proc. IEEE Position Location, Navig. Symp.*, San Diego, CA, Mar. 2000, pp. 185–192.
[30] G. Wahba, "Problem 65-1: A least squares estimate of satellite attitude," *SIAM Rev.*, vol. 7, no. 3, p. 409, Jul. 1965.
[31] T. Chin-Woo, S. Park, K. Mostov, and P. Varaiya, "Design of gyroscope-free navigation systems," in *Proc. IEEE Intell. Transport. Syst.*, Oakland, CA, Aug. 2001, pp. 286–291.
[32] W. T. Ang, P. K. Khosla, and C. Riviere, "Kalman filtering for real-time orientation tracking of handheld microsurgical instrument," in *Proc. IEEE Int. Conf. Intell. Robots Syst.*, Sendai, Japan, Sep. 2004, pp. 2574–2580.
[33] ——, "Design of all-accelerometer inertial measurement unit for tremor sensing in hand-held microsurgical instrument," in *Proc. IEEE Int. Conf. Robot. Autom.*, Taipei, Taiwan, Sep. 2003, vol. 2, pp. 1781–1786.
[34] E. Bachmann and X. Yun, "An investigation of the effects of magnetic variations on inertial/magnetic orientation sensors," *IEEE Robot. Autom. Mag.*, to be published.
[35] J. B. Kuipers, *Quaternions and Rotation Sequences*. Princeton, NJ: Princeton Univ. Press, 1999.
[36] J. L. Marins, "An extended Kalman filter for quaternion-based attitude estimation," Master's thesis, Naval Postgraduate School, Monterey, CA, Sep. 2000.
[37] M. D. Shuster and S. D. Oh, "Three-axis attitude determination for vector observations," *J. Guid. Control*, vol. 4, no. 1, pp. 70–77, 1981.
[38] G. Grenon, P. E. An, S. M. Smith, and A. J. Healey, "Enhancement of the inertial navigation system for the morpheus autonomous underwater vehicles," *IEEE J. Ocean. Eng.*, vol. 26, no. 4, pp. 548–560, Oct. 2001.

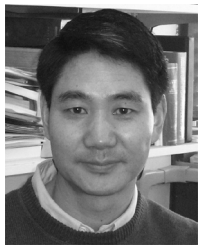

Xiaoping Yun (S'86–M'87–SM'96–F'05) received the B.S degree from Northeastern University, Shenyang, China in 1982, and the M.S. and D.Sc. degrees from Washington University, St. Louis, MO, in 1984 and 1987, respectively.

He is currently a Professor of Electrical and Computer Engineering at the Naval Postgraduate School, Monterey, CA. His research interests include coordinated control of multiple robotic manipulators, mobile manipulators, mobile robots, control of nonholonomic systems, MEMS sensors, carbon nanotubes-based sensors, and human body motion tracking using inertial/magnetic sensors.

Dr. Yun was an Associate Editor of the IEEE TRANSACTIONS ON ROBOTICS AND AUTOMATION from 1993 to 1996, and a Co-Editor of the Special Issue on "Mobile Robots" of the IEEE Robotics and Automation Society (RAS) Magazine in 1995. He was Co-Chair of the RAS Technical Committee on Mobile Robots in 1992–2003, a member of the RAS Conference Board in 1999–2003, a member of the Program Committee of the IEEE International Conference on Robotics and Automation in 1990, 1991, 1997, 1999, 2000, 2003, and 2004, a member of the Program Committee of the IEEE/RSJ International Conference on Intelligent Robots and Systems in 1998, 2001, 2003, and 2004, General Co-Chair of the 1999 IEEE International Symposium on Computational Intelligence in Robotics and Automation, Finance Chair of the IEEE International Conference on Robotics and Automation in 2002 and 2004, Finance Chair of the IEEE/RSJ International Conference on Intelligent Robots and Systems in 2001, 2004, 2005, and 2006, and Finance Chair of the IEEE International Conference on Nanotechnology in 2001. He is Treasurer of IEEE Robotics and Automation Society for 2004–2009, and was Vice President for Finance of the IEEE Nanotechnology Council in 2004–2006.

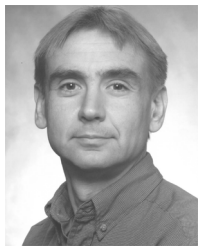

Eric R. Bachmann (M'01) received the Bachelors degree from the University of Cincinnati, Cincinnati, OH, and the M.S. and Ph.D. degrees from the Naval Postgraduate School, Monterey, CA.

He holds positions as an Associate Professor at Miami University, Oxford, OH, and as a Research Assistant Professor at the Naval Postgraduate School. Prior to this he served as an officer and an unrestricted naval aviator in the United States Navy. His research interests include inertial/magnetic human motion tracking, virtual environments, computer graphics, and visualization.